







## Photoelectrons as a Tracer of Planetary Atmospheric Composition: Application to CO on Mars

X.-S. Wu<sup>1,2</sup>, J. Cui<sup>2,3,4</sup> , R. V. Yelle<sup>5</sup> , Y.-T. Cao<sup>1,4</sup> , Z.-G. He<sup>2,3</sup> , F. He<sup>6,7</sup> , and Y. Wei<sup>6,7</sup> 

<sup>1</sup>National Astronomical Observatories, Chinese Academy of Sciences, Beijing, China, <sup>2</sup>Center for Excellence in Comparative Planetology, Chinese Academy of Sciences, Hefei, Anhui, China, <sup>3</sup>Planetary Environmental and Astrobiological Research Laboratory (PEARL), School of Atmospheric Sciences, Sun Yat-sen University, Zhuhai, Guangdong, China, <sup>4</sup>School of Astronomy and Space Sciences, University of Chinese Academy of Sciences, Beijing, China, <sup>5</sup>Lunar and Planetary Science Laboratory, University of Arizona, Tucson, Arizona, USA, <sup>6</sup>Institute of Geology and Geophysics, Chinese Academy of Sciences, Beijing, China, <sup>7</sup>School of Earth and Planetary Sciences, University of Chinese Academy of Sciences, Beijing, China

### Key Points:

- The altitude variation of photoelectron intensity at specific energies is a potential tracer of atmospheric composition
- The altitude variation of photoelectron intensity is controlled by the species-dependent inelastic electron impact cross section
- For Mars, a strong altitude variation of photoelectron intensity occurs at 10–15 eV and is sensitive to the CO abundance

### Correspondence to:

J. Cui,  
cuijun7@mail.sysu.edu.cn

### Citation:

X.-S. Wu, J. Cui, R. V. Yelle, Y.-T. Cao, Z.-G. He, & F. He, et al. (2020). Photoelectrons as a tracer of planetary atmospheric composition: Application to CO on Mars. *Journal of Geophysical Research: Planets*, 125, e2020JE006441. <https://doi.org/10.1029/2020JE006441>

Received 8 MAR 2020

Accepted 1 JUN 2020

Accepted article online 10 JUN 2020

**Abstract** Photoelectrons are an extensively studied component of planetary ionospheres which have been frequently used as a diagnostic of ambient magnetic fields. We show in this study that they also provide information on atmospheric composition via the altitude variation of photoelectron intensity at specific energies. Such an idea is applied to Mars for which a large observational sample of photoelectrons is available from the Solar Wind Electron Analyzer measurements made by the Mars Atmosphere and Volatile Evolution (MAVEN). Our analysis reveals a strong decline in photoelectron intensity from 160 to 200 km, but this trend is restricted to a narrow energy range of 10–15 eV. By employing analytical yield spectrum calculations, we derive the model variations based on different choices of the background atmosphere. We find that the presence of CO is crucial for reproducing the observed variations. This allows atmospheric CO densities to be estimated from photoelectron measurements, which are a factor of 3–7 lower than the published densities based on the MAVEN Neutral Gas and Ion Mass Spectrometer measurements and in better agreement with existing model results. In general, the usefulness of photoelectron intensity at a specific energy as a tracer of atmospheric composition relies critically on the species-dependent inelastic electron impact cross section at this energy.

**Plain Language Summary** On each solar system body with a substantial atmosphere, the ionization of atmospheric neutrals by solar photons produces photoelectrons at a typical energy of several eV to several hundred eV. These electrons have caught extensive research interests for decades because their spatial distribution has been recognized as a good tracer of ambient magnetic fields. In this study, we propose that photoelectrons could also be used as a tracer of atmospheric composition. Such an idea is applied to Mars, showing that the change of photoelectron flux with altitude at 10–15 eV relies critically on the distribution of atmospheric CO. When applied to other planets, the combination of the atmospheric species and photoelectron energy involved may vary, depending on the detailed characteristics of inelastic collisions between electrons and neutrals. Our idea provides a potentially useful constraint on the abundance of key atmospheric species when it cannot be measured accurately by a mass spectrometer, a situation often encountered in modern planetary missions.

### 1. Introduction

Photoelectrons are an extensively studied component of the dayside ionospheres of various solar system bodies such as the Earth (e.g., Doering et al., 1976), Mars (e.g., Frahm et al., 2006; Sakai et al., 2015), Venus (e.g., Coates et al., 2008; Cui et al., 2011), and Titan (e.g., Coates, 2007; Wellbrock et al., 2012), among others. It is well known that these nonthermal electrons are produced by solar extreme ultraviolet (EUV) and X-ray ionization of atmospheric neutrals (Fox et al., 2008). A typical photoelectron energy spectrum has a well-defined shape characterized by several distinctive spectral peaks at 22–27 eV connected to the strong solar He II emission line at 30.4 nm, as well as an apparent knee at 60–70 eV associated with the rapid drop in solar flux at wavelengths shorter than 17 nm (Coates, 2011, and references therein).

Photoelectrons are important in at least two aspects. On the one hand, they are able to ionize ambient neutrals and heat ambient thermal electrons, hence playing an important role in the local ionization

and energy balance (e.g., Cui et al., 2018; Galand et al., 2006; Sakai et al., 2016). On the other hand, they are frequently observed in regions where local photoelectron production is not expected, and accordingly, they are used as a diagnostic of the ambient magnetic field topology (e.g., Cao et al., 2020; Coates, 2007, 2015; Xu et al., 2017). One may also expect that a photoelectron spectrum contains information on the composition of the background atmosphere because species-dependent ionization potential would naturally cause species-dependent location of the spectral peak. However, this fact is of little practical use because the typical energy resolution of a measured photoelectron spectrum, at the order of several eV, is too coarse to distinguish between peaks associated with different species such as CO<sub>2</sub> and O on Mars and Venus, with an energy difference of only 0.2 eV. Despite this, we show below that photoelectrons can indeed be used as a potential tracer of the background atmospheric composition in the optically thin regions, not by identifying separated peaks but by examining the altitude variation of photoelectron intensity.

In this paper, such an idea is explained and applied specifically to Mars, which is ideally suited for a systematic investigation of the characteristics of ionospheric photoelectrons as allowed by the accumulation of numerous photoelectron energy spectra over the past few decades by a number of instruments including the Magnetometer/Electron Reflectometer (MAG/ER) on board the Mars Global Surveyor (MGS) (Mitchell et al., 2001), the Electron Spectrometer as a part of the Analyzer of Space and Energetic Atoms on board the Mars Express (Frahm et al., 2006), and more recently the Solar Wind Electron Analyzer (SWEA) on board the Mars Atmosphere and Volatile Evolution (MAVEN) mission (Mitchell et al., 2016). For instance, based on the MGS MAG/ER data, Xu et al. (2016) found that the photoelectron intensity was correlated with solar EUV and X-ray flux but independent of solar zenith angle (SZA). Using the MAVEN SWEA data, Wu, Cui, Cao, Liu, et al. (2019) analyzed the shape of the photoelectron energy spectrum, revealing systematic trends with altitude and SZA. The SWEA data are unique among existing measurements near Mars in that they provide the only opportunity so far to explore photoelectrons down to the ionospheric peak altitude (e.g., Jakosky et al., 2015).

The paper is organized as follows. In section 2, we present SWEA observations which reveal a strong altitude variation of photoelectron intensity at specific energies even within the optically thin regions of the Martian atmosphere. Data-model comparison is presented in section 3, where we highlight the crucial role of CO in determining the observed variation. We then discuss in section 4 what is special for CO and provide concluding remarks in section 5.

## 2. Clues from the MAVEN Measurements at Mars

For the purpose of this study, we show in Figure 1a the mean photoelectron energy spectrum as a function of altitude based on the SWEA measurements gathered during the Deep Dip (DD) campaign in April 2015, hereafter denoted as DD2 for short, with a periapsis altitude of 130–135 km and a periapsis SZA of 8° to 12°. The displayed spectrum has been corrected for spacecraft charging using the appropriate potentials provided in the MAVEN Neutral Gas and Ion Mass Spectrometer (NGIMS) level 2 data set (Mahaffy et al., 2015). The figure demonstrates clearly the presence of a distinctive peak near 22–27 eV, along with the sharp decline in photoelectron intensity beyond 60 eV.

Of particular interest is the altitude variation of photoelectron intensity, which is displayed in Figure 1b at several representative energies, where the measured intensity has been normalized by the value at 200 km to facilitate cross energy comparison of the overall trend. We focus on the altitude range from the DD2 periapsis to 200 km where the condition of local energy degradation could be reasonably assumed for the observed photoelectrons (e.g., Wu, Cui, Cao, Sun, et al., 2019). Two broad categories are immediately identified in the figure: (1) At relatively high energies, the photoelectron intensity remains roughly constant with altitude down to 140–150 km below which it declines with decreasing altitude; (2) at relatively low energies, the photoelectron intensity is peaked at an altitude of around 160 km and declines toward both lower and higher altitudes. Based on the SWEA measurements made at other energies up to 250 eV (above which the contribution from solar wind electrons is a concern), we conclude that the former feature is persistently seen above 15 eV, whereas the latter feature is restricted to a narrow energy range of 10–15 eV. Dayside SWEA measurements down to the ionospheric peak altitude are also available from another DD campaign in October 2017, with a periapsis altitude of 122–137 km and a periapsis SZA of 21° to 28°. Without showing the details, we mention that very similar observations are revealed by the SWEA measurements from this

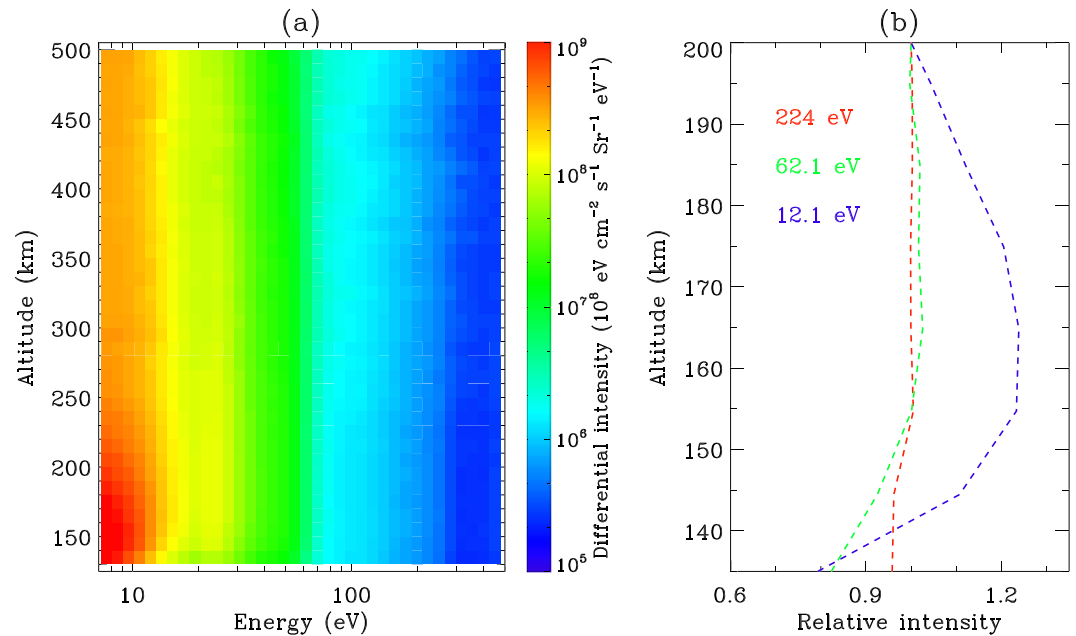


**Figure 1.** (a) The mean photoelectron intensity as a function of altitude and energy based on the MAVEN SWEA measurements during the Deep Dip campaign in April 2015. (b) The altitude variation of photoelectron intensity at several representative energies (indicated in the figure legend), where the measured intensity has been normalized by the value at 200 km to facilitate cross energy comparison of the overall trend.

extra campaign. In addition, by scrutinizing a substantially larger SWEA data set during the nominal MAVEN mission phase (which typically probed the Martian atmosphere down to 150–160 km only), we conclude that the energy-dependent altitude variations above 160 km as seen in Figure 1b are fairly common on the dayside of Mars.

The decline in photoelectron intensity toward the DD2 periapsis at all energies is clearly attributed to the attenuation of solar EUV and X-ray irradiance due to photoabsorption by neutrals near and below the ionospheric peak, which is at around 130 km under the subsolar condition (e.g., Fox & Weber, 2012; Morgan et al., 2008; Yao et al., 2019). In Figure 1b, the observation of a less prominent decline in photoelectron intensity at higher energies reflects the ability of more energetic photons to penetrate deeper into the atmosphere (e.g., Fox, 2004). In contrast, the strong altitude variation of photoelectron intensity above 160 km, which is only seen at 12.1 eV in the figure and by as much as 25% up to 200 km, is counterintuitive.

Assuming local energy degradation, photoelectrons at a given energy are, as a first-order approximation, produced via solar EUV and X-ray ionization and lost via inelastic collisions with ambient neutrals (e.g., Fox et al., 2008). Since both the photoelectron production and loss rates are proportional to the ambient neutral density, one may intuitively expect that the photoelectron intensity is independent of altitude within the optically thin regions where the attenuation in solar EUV and X-ray irradiance is negligible (as is the case for the 224- and 62.1-eV photoelectrons above 160 km in Figure 1b). We note that such a simple argument only applies to the situation of a single component atmosphere, and we show below that the counterintuitive altitude variation in the optically thin regions at 10–15 eV reflects in reality how the ambient atmosphere is mixed by different neutral species with different characteristics of the inelastic electron impact cross section.

### 3. Analytical Yield Spectrum Modeling Results

For the altitude range displayed in Figure 1b, the condition of local energy degradation is a reasonable approximation (e.g., Wu, Cui, Cao, Sun, et al., 2019), which facilitates greatly the calculation of the photoelectron intensity in the Martian ionosphere with the aid of the analytical yield spectrum (AYS) method. Such a method was recently used by Mukundan et al. (2020), who reported a good agreement between the model photoelectron spectra and the SWEA measurements over the energy range of 10–250 eV

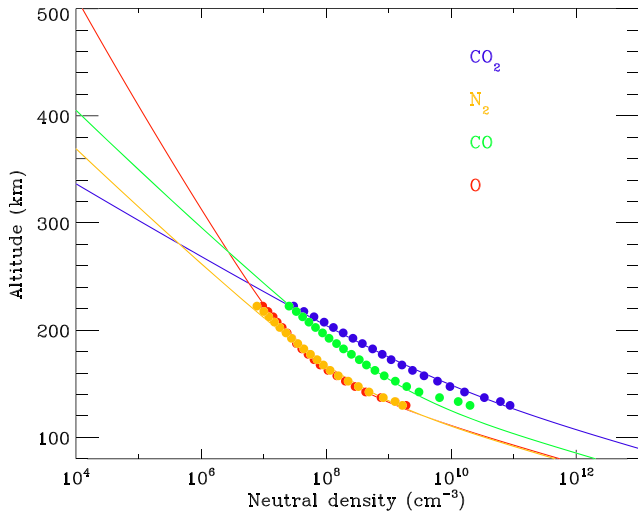


**Figure 2.** The background Martian atmosphere at 80–500 km including CO<sub>2</sub>, O, N<sub>2</sub>, and CO as given by the solid lines. The MAVEN NGIMS measurements averaged over all inbound DD2 orbits are given by the solid circles for validation.

without the need to adjust the solar EUV and X-ray irradiance inferred from the MAVEN Extreme Ultraviolet Monitor band irradiance data (Thiemann et al., 2017). The AYS method has the advantage of isolating the nonspatial information of the photoelectron degradation processes and incorporating photoelectron production via downward degradation from more energetic states with a parametrized two-dimensional matrix (Green et al., 1977). Degradation via Coulomb collisions with ionospheric thermal electrons (Stamnes & Rees, 1983) is only important for photoelectron energy well below 10 eV and is ignored for simplicity.

The background Martian atmosphere required for AYS model calculations is depicted in Figure 2, including the neutral density profiles of CO<sub>2</sub>, O, N<sub>2</sub>, and CO from 80 to 500 km. These profiles are validated by the MAVEN NGIMS measurements averaged over DD2 (Mahaffy et al., 2015), as displayed in the same figure for comparison. Only the inbound NGIMS data are used to avoid possible contamination by heterogenous chemistry as well as physical adsorption and desorption occurring on the instrument antechamber walls (e.g., Mahaffy et al., 2015). For reference, we explain in detail in Appendix A how the background atmosphere is constructed.

Following Mukundan et al. (2020), we compute the photoelectron intensity,  $\Phi_e(E, z)$ , as a function of altitude,  $z$ , and energy,  $E$ , from

$$\Phi_e(E, z) = \frac{\int_E^\infty P_e(z, E') Y_c(E, E', z) dE'}{\sum_i N_i(z) \sigma_i(E)}, \quad (1)$$

where  $N_i$  is the density of neutral species,  $i$ ,  $\sigma_i$  is the total inelastic electron impact cross section,  $P_e$  is the differential photoelectron production rate by solar EUV and X-ray ionization of all neutral species, and  $Y_c$  is the composite AYS obtained with

$$Y_c(E, E', z) = \frac{\sum_i N_i(z) \langle \sigma_i(E, E') \rangle Y_i(E, E')}{\sum_i N_i(z) \langle \sigma_i(E, E') \rangle}, \quad (2)$$

with  $\langle \sigma_i \rangle$  being  $\sigma_i$  averaged over the energy range of  $E$  to  $E'$  and  $Y_i$  being the respective AYS for neutral species,  $i$ , characterizing the production of photoelectrons at  $E$  from downward degradation of photoelectrons at  $E'$ . For  $Y_i$ , we adopt the results of Green et al. (1977) for all species except for CO<sub>2</sub> for which the more accurate result of Bhardwaj and Jain (2009) is used. The latter result accounts for the serious underestimates of the CO<sub>2</sub> AYS by earlier results near and below 15 eV (see Figure 6 of Bhardwaj & Jain, 2009).

In Figure 3a, we show the model altitude variation of photoelectron intensity at the same representative energies as in Figure 1b using the background atmosphere depicted in Figure 2. The model variation in Figure 3a is in rough agreement with the observed variation. The two broad categories are clearly identified in that above 160 km, the photoelectron intensity varies little with altitude at relatively high energies but shows distinctive decline with increasing altitude at the lowest energy of 12.1 eV displayed in the figure, just as suggested by the SWEA measurements. In our calculations, the input solar EUV and X-ray irradiance is adopted from the Flare Irradiance Spectral Model - Mars (Thiemann et al., 2017) appropriate for the DD2 condition, with the respective mean SZA of 11°. The relevant photoionization cross sections are taken from Masuoka (1994) for CO<sub>2</sub>, Verner et al. (1996) for O, Stolte et al. (1998) for N<sub>2</sub>, and Masuoka and Nakamura (1993) for CO.

It is also instructive to make data-model comparison when the neutral density profiles are modified arbitrarily in order to explore the effect of a varying background atmosphere. For this purpose, we show in Figure 3b the model variation by including CO<sub>2</sub> only, indicating that the photoelectron intensity is now

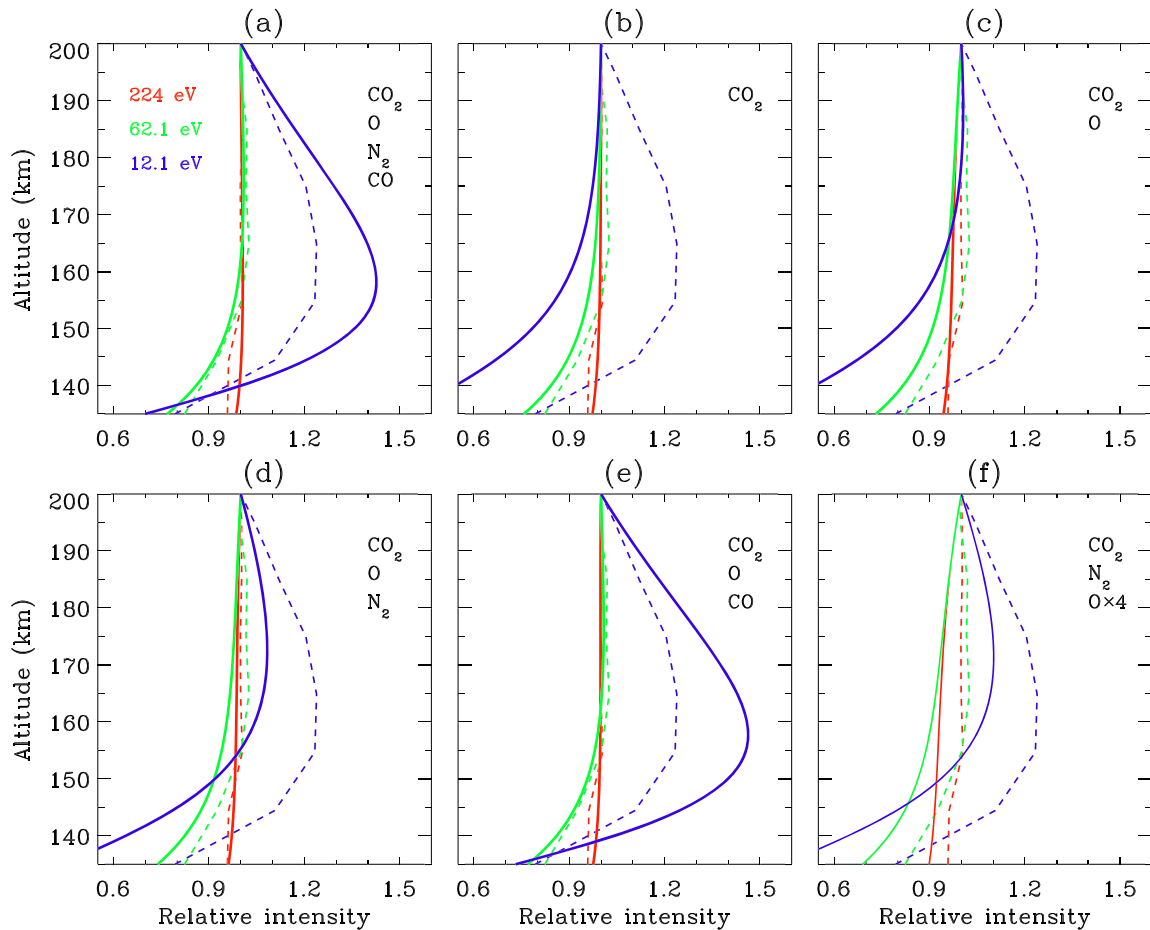


**Figure 3.** The altitude variation of photoelectron intensity at several representative energies (indicated in the figure legend in panel (a)) according to our AYS model calculations, in a similar format as in Figure 1b. The SWEA observations are given by the dashed lines for comparison. Different model runs are indicated assuming different choices of the background Martian atmosphere including CO<sub>2</sub>, O, N<sub>2</sub>, and CO (a), CO<sub>2</sub> only (b), CO<sub>2</sub> and O (c), CO<sub>2</sub>, O, and N<sub>2</sub> (d), and CO<sub>2</sub>, O, and CO (e), all in agreement with the NGIMS measurements, as well as an additional background atmosphere including CO<sub>2</sub>, O, and N<sub>2</sub> for which the CO<sub>2</sub> and N<sub>2</sub> densities are in agreement with the NGIMS measurements but the O densities are enhanced by a factor of 4 as suggested by Fox et al. (2017) (f).

altitude independent in the optically thin regions irrespective of energy, as suggested by the ideal expectation described in section 2. As several additional model runs, we show the same variation when including CO<sub>2</sub> and O only in Figure 3c, when including CO<sub>2</sub>, O, and N<sub>2</sub> only in Figure 3d, and when including CO<sub>2</sub>, O, and CO only in Figure 3e, respectively. A final model run is depicted in Figure 3f, for which we include CO<sub>2</sub>, O, and N<sub>2</sub> only but with the O densities in Figure 2 enhanced by a factor of 4 at all altitudes following the suggestion of Fox et al. (2017).

A comparison of different model runs indicates that the observed altitude variation of photoelectron intensity at 10–15 eV strongly relies on the detailed atmospheric composition. Based on the NGIMS measurements, CO makes the second most important contribution to the ambient atmosphere over the altitude range of 160–200 km examined here, where its density is on average higher than the O density by a factor of around 4 according to Figure 2. The SWEA data suggest a significant decline in photoelectron intensity from 160 to 200 km at 12.1 eV. Though containing the same CO<sub>2</sub>, O, and N<sub>2</sub> density profiles as in model (a), model (d) does not reproduce the same feature when the background atmosphere does not include CO. Enhancing the O density profile, as done for model (f), does not help to solve the problem. In practice, even if we enhance the O density everywhere by an unrealistically large factor of 10 for a pure CO<sub>2</sub> and O atmosphere (not shown in the figure), the predicted altitude variation of photoelectron intensity at 12.1 eV is only 5% at 160–200 km. The SWEA observations at 12.1 eV do not appear to be linked to N<sub>2</sub> as

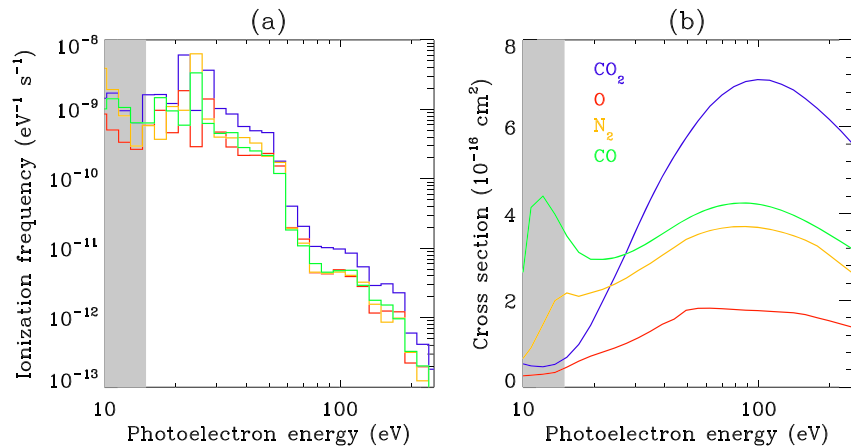


**Figure 4.** (a) The energy-dependent photoionization frequencies of various species at a reference altitude of 180 km in the Martian upper atmosphere (see Figure 2). (b) The total inelastic electron impact cross sections of various species. The shaded regions in both panels refer to the energy range of 10–15 eV over which a strong altitude variation of photoelectron intensity at 160–200 km is suggested by the MAVEN SWEA measurements during DD2.

well because model (e), despite without  $N_2$  in the background atmosphere, does predict the observed variation, at least qualitatively. Following the above discussions, we conclude that the observed altitude variation of photoelectron intensity at 10–15 eV strongly relies on the detailed atmospheric composition. Especially, CO appears to play an essential role in that all model runs without this species fail to reproduce adequately the observed variation for low energy photoelectrons.

#### 4. Discussion: The Role of Atmospheric CO on Mars

According to Equation 1, the photoelectron intensity is determined by photoionization and energy degradation via inelastic collisions, both of which depend on the atmospheric composition. Here we compare in Figure 4a the photoionization frequencies of various species at a reference altitude of 180 km. The figure reveals a comparable ability between  $CO_2$  and CO to produce photoelectrons at 10–15 eV by solar EUV and X-ray ionization.

In contrast, the two species do show a clear distinction in the total inelastic electron impact cross section, as displayed in Figure 4b based on the cross sections reported by Itikawa (2002) for  $CO_2$ , Laher and Gilmore (1990) for O, Itikawa (2006) for  $N_2$ , and Brunger and Buckman (2002) for CO, respectively. At 10–15 eV, the CO cross section is larger than the  $CO_2$  cross section, implying an easier loss of 10- to 15-eV photoelectrons via inelastic collisions with CO than with  $CO_2$ . This is compatible with the observed altitude variation at 10–15 eV in Figure 1b, when combined with the NGIMS observation that from 160 to 200 km, the CO mixing ratio increases significantly from 15% to 30% in the Martian upper atmosphere (however, see below). Such an effect is exceptionally prominent due to the large cross section difference between the two species by a factor of 8. Enhanced inelastic electron collisions with CO at 10–15 eV are mainly connected to electronic excitation to either the  $a^3\Pi$  state or the  $a'^3\Sigma$  state of CO, with excitation energies of 6.22 and 6.91 eV, respectively (e.g., Brunger & Buckman, 2002).

Meanwhile, the  $CO_2$  cross section is larger than the CO cross section above 27 eV according to Figure 4b. This implies that the 10- to 15-eV photoelectrons are more easily produced by downward degradation of more energetic photoelectrons via inelastic collisions with  $CO_2$  than with CO. Obviously this also contributes to the observed decline in photoelectron intensity at 10–15 eV above 160 km though to a less extent.

For further demonstration, we show in Figure 5 the altitude profiles of the NGIMS CO mixing ratio, the primary photoelectron production rate, the composite AYS defined in Equation 2, and the mean inelastic electron impact cross section of atmospheric neutrals weighted by mixing ratio. The situations for two photoelectron energies, 12.1 and 38.9 eV, are compared to highlight the differences in various controlling parameters between the two categories of photoelectron observation with and without a prominent

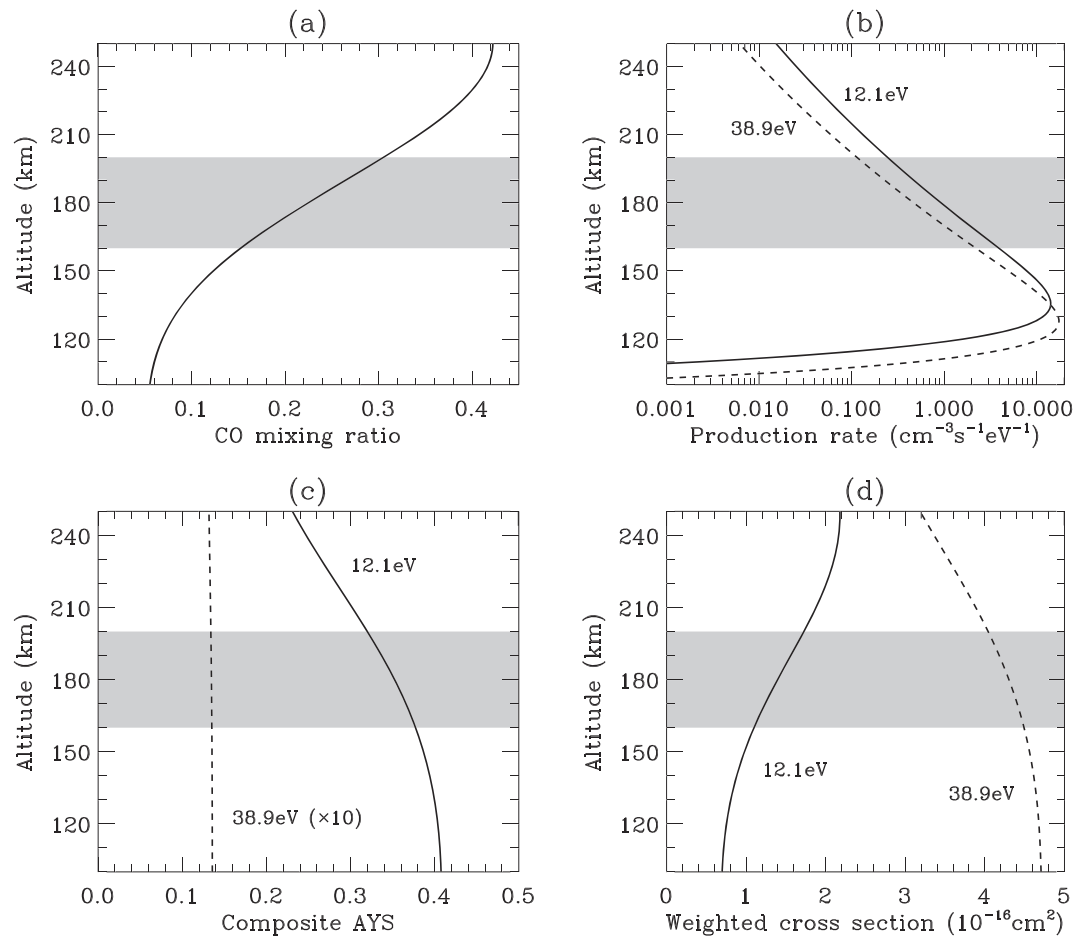


**Figure 5.** The altitude profiles of the NGIMS CO mixing ratio (a), the primary photoelectron production rate (b), the composite AYS defined in Equation 2 (c), and the mean inelastic electron impact cross section of atmospheric neutrals weighted by mixing ratio (d). Except for panel (a), the solid and dashed lines refer to the 12.1 eV and 38.9 eV photoelectrons, respectively. In panel (c), the composite AYS refers to downward degradation of photoelectrons from a representative upper energy state of 124.9 eV. Note also that the composite AYS at 38.9 eV has been multiplied by 10 to improve visibility. The shaded region in each panel encompasses the altitude range of 160–200 km where a prominent decline in photoelectron intensity with increasing altitude is revealed by the SWEA measurements of 10–15 eV photoelectrons.

decline in photoelectron intensity at 160–200 km (indicated by the shaded region in each panel). Figure 5b suggests a similar altitude trend in primary photoelectron production at the two energies, whereas Figures 5c and 5d reveal that the altitude trends of photoelectron production and loss via downward energy degradation are remarkably different between 12.1 and 38.9 eV. When the CO mixing ratio increases with increasing altitude, photoelectron loss at 12.1 eV via downward degradation to less energetic states increases whereas photoelectron production at the same energy via downward degradation from more energetic states decreases. The combination of the above two effects accounts for the observed decline in photoelectron intensity at 12.1 eV with increasing altitude.

Analogous to CO, we note that the total inelastic electron impact cross section of  $\text{N}_2$  is also larger than that of  $\text{CO}_2$  at 10–15 eV but only by a factor of 3 according to Figure 4b. This explains why a weaker altitude variation (by less than 10%) of photoelectron intensity at these energies is predicted by the model run in Figure 4d that includes  $\text{CO}_2$ , O, and  $\text{N}_2$  but does not include CO in the background atmosphere. Meanwhile, no enhancement in the total inelastic electron impact cross section is seen for O at 10–15 eV, which is consistent with no altitude variation of photoelectron intensity for a background atmosphere containing only  $\text{CO}_2$  and

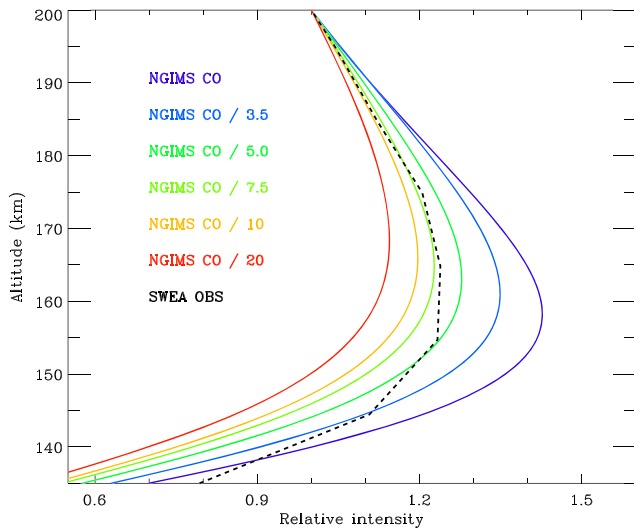


**Figure 6.** Similar to Figure 3, the altitude variation of photoelectron intensity at 12.1 eV predicted by AYS model calculations assuming different background atmospheres with identical CO<sub>2</sub>, N<sub>2</sub>, and O density profiles based on direct NGIMS measurements but different CO density profiles as indicated in the figure legend. The altitude variation inferred from the SWEA measurements during DD2 is superimposed for comparison.

O as presented in Figure 3c. In general, the altitude variation of photoelectron intensity at a specific energy is crucially controlled by the species-dependent inelastic collisions by photoelectrons at the same energy.

The above discussion implies that it is possible to infer planetary atmospheric composition from the measured photoelectron intensities at selected energies. This is especially interesting for the case of CO in the Martian upper atmosphere since the densities of this species are not well constrained by the NGIMS measurements. It is known that the O densities directly measured by the NGIMS are strongly affected by the recombination of atmospheric O on the chamber walls to form O<sub>2</sub> (Stone et al., 2018). Similarly, the NGIMS NO densities have been proposed to be linked to the recombination of atmospheric O and N on the chamber walls rather than reflecting the amount of atmospheric NO (Stevens et al., 2019). The latter is also supported by the recent investigation of odd N chemistry in the Martian upper atmosphere by Cui et al. (2020). However, the situation for CO is quite different because the recombination of atmospheric C and O on the chamber walls makes a small contribution to the measured count rates compared to the direct contribution from atmospheric CO. In reality, the uncertainty in the NGIMS CO density is due to the fact that the CO count rates are seriously contaminated by CO<sub>2</sub> and N<sub>2</sub> whose cracking patterns are not known accurately enough to allow a robust determination of the atmospheric CO density.

Here several AYS model runs are carried out, as displayed in Figure 6 where we show the model altitude variation of photoelectron intensity at 12.1 eV for different background atmospheres characterized by different CO density profiles as indicated in the figure legend. The density profiles of the other three species, CO<sub>2</sub>, N<sub>2</sub>, and O, are based on direct NGIMS measurements. The figure demonstrates that a reduction of CO density everywhere by a factor of 3–7 relative to the NGIMS density reproduces reasonably the observed altitude variation of photoelectron intensity. At 160 km, the CO density is  $7 \times 10^8 \text{ cm}^{-3}$  according to direct NGIMS measurements whereas a comparison between AYS model results and SWEA observations suggests that this density might be substantially overestimated and that a more likely CO density is  $(1\text{--}2) \times 10^8 \text{ cm}^{-3}$  at 160 km. The revised CO density profile agrees better with existing model predictions (e.g., Krasnopolsky, 2002, 2010). It is also interesting to note that the NGIMS NO densities are proposed to be overestimated by a comparable factor (e.g., Cui et al., 2020).

The above simple calculations should be regarded as a demonstration of the possibility to constrain atmospheric composition and structure from photoelectron intensity measurements, rather than an attempt to accurately reproduce the data. For instance, the data-model comparison in Figure 6 suggests clearly that applying a common scaling factor for CO density is not able to reproduce the SWEA observations at all altitudes. The data-model agreement is expected to be improved by more sophisticated multi-stream calculations that include the effect of photoelectron transport along the magnetic field lines, which we leave for follow-up studies.

## 5. Concluding Remarks

Photoelectrons are an extensively studied nonthermal component of planetary ionospheres with a typical energy of several eV to several  $10^2$  eV (e.g., Coates, 2011). While these electrons have been frequently used as a diagnostic of the ambient magnetic field topology (e.g., Cao et al., 2020; Coates, 2007, 2015; Xu et al., 2017), we show further in this study that they also provide interesting information on the ambient atmospheric composition within the optically thin regions, in terms of the altitude variation of photoelectron intensity at specific energies.

The above idea is applied to Mars for which the MAVEN SWEA measurements have provided, over the past few years, an exceptionally large data set of photoelectrons down to the ionospheric peak altitude

(Mitchell et al., 2016). Based on the SWEA data acquired during DD2 appropriate for the subsolar condition, we find a strong decline in photoelectron intensity from 160 to 200 km, but this trend is restricted to a narrow photoelectron energy range of 10–15 eV. At higher energies, the photoelectron intensity is fairly constant above 160 km, which is consistent with the ideal expectation for a single component atmosphere because both the photoelectron production and loss rates are proportional to the ambient neutral density, leaving no net effect exerted by the background atmosphere.

By employing simple AYS model calculations (e.g., Mukundan et al., 2020), we derive the altitude variation of photoelectron intensity at representative energies based on different choices of the background atmosphere. We find that the presence of CO is crucial for reproducing the observations, and such an interesting finding is mainly due to enhanced inelastic collisions of photoelectrons with CO at 10–15 eV when compared to collisions with CO<sub>2</sub> (Brunger & Buckman, 2002). An easier production of 10- to 15-eV photoelectrons by downward degradation of more energetic photoelectrons via inelastic collisions with CO<sub>2</sub> than with CO (Bhardwaj & Jain, 2009; Green et al., 1977) also contributes to the observed altitude variation at 160–200 km, though to a less extent. The AYS model results cannot be extrapolated to higher altitudes where the effect of transport becomes important.

We propose that the altitude variation of photoelectron intensity at 10–15 eV could be used as a tracer of CO in the Martian upper atmosphere. Following a similar line of reasoning, we may further conclude that the same variation is not sensitive to the abundances of atmospheric N<sub>2</sub> and O on Mars because their inelastic electron impact cross sections are not substantially enhanced over that of CO<sub>2</sub> at 10–15 eV (Itikawa, 2006; Laher & Gilmore, 1990). The CO densities in the Martian upper atmosphere as directly measured by the NGIMS are likely very uncertain. Therefore, as an application of the idea described here, we carry out a set of AYS model runs with fixed CO<sub>2</sub>, N<sub>2</sub>, and O density profiles but a variable CO density profile in order to constrain the possible range of CO density that reproduces the SWEA observations near a representative photoelectron energy of 12 eV. The data-model comparison indicates that the NGIMS CO densities are likely overestimated by a large factor of 3–7 in the Martian upper atmosphere.

In practice, the usefulness of photoelectron intensity at a specific energy as a tracer of atmospheric composition relies crucially on the species-dependent inelastic collisions by photoelectrons at the same energy. The idea outlined in the present paper is potentially useful either for a planetary mission without a neutral mass spectrometer but with an electron spectrometer on board such as the Venus Express (Coates et al., 2008) or when the mass spectrometer does not provide an accurate determination of an ambient species (Mahaffy et al., 2015).

### Appendix A: Construction of the Background Martian Atmosphere

The background Martian atmosphere used in the AYS model calculation is displayed in Figure 2, including CO<sub>2</sub>, O, N<sub>2</sub>, and CO. The CO<sub>2</sub> density profile is obtained from the hydrostatic balance equation with a neutral temperature profile,  $T(z)$ , analogous to that of Krasnopolsky (2002) in the form of

$$T(z) = T_{\infty} - (T_{\infty} - T_0) \exp \left[ -\frac{(z-z_0)^2}{22T_{\infty}} \right], \quad (\text{A1})$$

with  $T_{\infty} = 245$  K from isothermal fitting to the NGIMS CO<sub>2</sub> data above 160 km,  $T_0 = 140$  K at the lower boundary of  $z_0 = 80$  km according to the recent Mars Climate Sounder limb observations made on board the Mars Reconnaissance Orbiter (Kleinböhl et al., 2009), and the numerical factor of 22 constrained by comparing the derived CO<sub>2</sub> densities with the NGIMS data.

The density profile of each of the remaining species is described by the respective momentum equation taking into account both eddy diffusion and molecular diffusion. Here the eddy diffusion coefficient,  $K(z)$ , is parameterized with the functional form of Krasnopolsky (2002) as

$$K(z) = K_0 \sqrt{\frac{T_{\infty}}{N_{\text{CO}_2}(z)}}, \quad (\text{A2})$$

where  $N_{\text{CO}_2}$  is the  $\text{CO}_2$  density and  $K_0 = 3.27 \times 10^{11} \text{ cm}^2 \text{ s}^{-1}$  is constrained by the NGIMS  $\text{N}_2$  data assuming diffusive equilibrium (e.g., Slipski et al., 2018). With this, the CO density profile is then favorably determined also assuming diffusive equilibrium. The departure in CO density near and below 140 km is likely due to nonnegligible CO production from various photochemical pathways, but such a departure is unimportant because we are interested in the regions above 160 km where the data-model agreement in Figure 2 is fairly good for CO.

For O, we find that the condition of diffusive equilibrium is inappropriate and an extremely large upward flux of  $3 \times 10^{10} \text{ cm}^{-2} \text{ s}^{-1}$  is required to reproduce the NGIMS measurements. Despite orders of magnitude higher than the atomic O escape flux, known to be primarily driven by the dissociative recombination of ionospheric  $\text{O}_2^+$  (e.g., Lillis et al., 2017), such a large flux may not be totally unrealistic considering that it may reflect a strong ballistic flow that emanates from the subsolar regions of Mars and forms a very extended corona as revealed by existing remote sensing observations (e.g., Chaufray et al., 2015). We also caution that the NGIMS O densities have been speculated to be inaccurate by Fox et al. (2017), and more sophisticated model calculations are required to confirm this speculation.

The background atmosphere can be accessed via Cui, Jun; Wu, Xiaoshu (2020), Photoelectrons as a Tracer of Planetary Atmospheric Composition: Application to CO on Mars; Mendeley Data, V1, (<https://doi.org/10.17632/4zy92xgf45.1>).

### Data Availability Statement

The data used in this work are publicly available at the MAVEN Science Data Center (<http://lasp.colorado.edu/maven/sdc/public/>). The IDL procedures used to do all the calculations presented in this study and the data files required for making all the figures are accessible via Cui, Jun; Wu, Xiaoshu (2020), Photoelectrons as a tracer of planetary atmospheric composition: Application to CO on Mars, Mendeley Data, V1, (<https://doi.org/10.17632/4zy92xgf45.1>).

### Acknowledgments

This work is supported by the B-type Strategic Priority Program No. XDB41000000 funded by the Chinese Academy of Sciences and the pre-research project on Civil Aerospace Technologies No. D020105 funded by China's National Space Administration. The authors also acknowledge supports from the National Science Foundation of China (NSFC) through grants 41904154, 41525015, 41774186, and 41525016. The authors thank Robert Lillis and the other anonymous referees for their constructive comments which have improved the quality of the manuscript substantially.

### References

- Bhardwaj, A., & Jain, S. K. (2009). Monte Carlo model of electron energy degradation in a  $\text{CO}_2$  atmosphere. *Journal of Geophysical Research*, *114*, A11309. <https://doi.org/10.1029/2009JA014298>
- Brunger, M. J., & Buckman, S. J. (2002). Electron-molecule scattering cross-sections. I. Experimental techniques and data for diatomic molecules. *Physics Reports*, *357*, 215.
- Cao, Y.-T., Caro Carretero, R., & Wellbrock, A. (2020). Field-aligned photoelectron energy peaks at high altitude and on the nightside of Titan. *Journal of Geophysical Research: Planets*, *125*, e2019JE006252. <https://doi.org/10.1029/2019JE006252>
- Chaufray, J. Y., Deighan, J., Chaffin, M. S., Schneider, N. M., McClintock, W. E., Stewart, A. I. F., et al. (2015). Study of the Martian cold oxygen corona from the OI 130.4 nm by IUVS/MAVEN. *Geophysical Research Letters*, *42*, 9031–9039. <https://doi.org/10.1002/2015GL065341>
- Coates, A. J., Crary, F. J., Young, D. T., Szego, K., Arridge, C. S., Bebesi, Z., et al. (2007). Ionospheric electrons in Titan's tail: Plasma structure during the Cassini T9 encounter. *Geophysical Research Letters*, *34*, L24S05. <https://doi.org/10.1029/2007GL030919>
- Coates, A. J., Tsang, S. M. E., Wellbrock, A., Frahm, R. A., Winningham, J. D., Barabash, S., et al. (2011). Ionospheric photoelectrons: Comparing Venus, Earth, Mars and Titan. *Planetary and Space Science*, *59*, 1019–1027.
- Coates, A. J., Wellbrock, A., Frahm, R. A., Winningham, J. D., Fedorov, A., Barabash, S., & Lundin, R. (2015). Distant ionospheric photoelectron energy peak observations at Venus. *Planetary and Space Science*, *113*, 378–384.
- Coates, A. J., Crary, F. J., Young, D. T., Szego, K., Arridge, C. S., Bebesi, Z., et al. (2008). Ionospheric photoelectrons at Venus: Initial observations by ASPERA-4 ELS. *Planetary and Space Science*, *56*, 802.
- Cui, J., Fu, M. H., Ren, Z. P., Gu, H., Wu, X. S., et al. (2020). Nitric oxide abundance in the Martian thermosphere and its diurnal variation. *Geophysical Research Letters*, *47*, e87252. <https://doi.org/10.1029/2020GL087252>
- Cui, J., Galand, M., Coates, A. J., Zhang, T. L., & Müller-Wodarg, I. C. F. (2011). Suprathermal electron spectra in the Venus ionosphere. *Journal of Geophysical Research*, *116*, A04321. <https://doi.org/10.1029/2010JA016153>
- Cui, J., Wu, X.-S., Xu, S.-S., Wang, X.-D., Wellbrock, A., Nordheim, T. A., et al. (2018). Ionization efficiency in the dayside Martian upper atmosphere. *The Astrophysical Journal*, *857*, L18.
- Doering, J. P., Peterson, W. K., Bostrom, C. O., & Potemra, T. A. (1976). High resolution daytime photoelectron energy spectra from AE-E. *Geophysical Research Letters*, *3*(3), 129–131.
- Fox, J. L. (2004). Response of the Martian thermosphere/ionosphere to enhanced fluxes of solar soft X rays. *Journal of Geophysical Research*, *109*, A11310. <https://doi.org/10.1029/2004JA010380>
- Fox, J. L., Galand, M. I., & Johnson, R. E. (2008). Energy deposition in planetary atmospheres by charged particles and solar photons. *Space Science Reviews*, *139*, 3.
- Fox, J. L., Johnson, A. S., Ard, S. G., Shuman, N. S., & Viggiano, A. A. (2017). Photochemical determination of O densities in the Martian thermosphere: Effect of a revised rate coefficient. *Geophysical Research Letters*, *44*, 8099–8106. <https://doi.org/10.1002/2017GL074562>
- Fox, J. L., & Weber, A. J. (2012). MGS electron density profiles: Analysis and modeling of peak altitudes. *Icarus*, *221*, 1002.
- Frahm, R. A., Sharber, J. R., Winningham, J. D., Wurz, P., Liemohn, M. W., Kallio, E., et al. (2006). Locations of atmospheric photoelectron energy peaks within the Mars environment. *Space Science Reviews*, *126*, 389.

- Galand, M., Yelle, R. V., Coates, A. J., Backes, H., & Wahlund, J.-E. (2006). Electron temperature of Titan's sunlit ionosphere. *Geophysical Research Letters*, *33*, L21101. <https://doi.org/10.1029/2006GL027488>
- Green, A. E. S., Jackman, C. H., & Garvey, R. H. (1977). Electron impact on atmospheric gases, 2. Yield spectra. *Journal of Geophysical Research*, *82*, 5104.
- Itikawa, Y. (2002). Cross sections for electron collisions with carbon dioxide. *Journal of Physical and Chemical Reference Data*, *31*, 749.
- Itikawa, Y. (2006). Cross sections for electron collisions with nitrogen molecules. *Journal of Physical and Chemical Reference Data*, *35*, 31.
- Jakosky, B. M., Grebowsky, J. M., Luhmann, J. G., & Brain, D. A. (2015). Initial results from the MAVEN mission to Mars. *Geophysical Research Letters*, *42*, 8791–8802. <https://doi.org/10.1002/2015GL065271>
- Kleinböhl, A., Schofield, J. T., Kass, D. M., Abdou, W. A., Backus, C. R., Sen, B., et al. (2009). Mars Climate Sounder limb profile retrieval of atmospheric temperature, pressure, and dust and water ice opacity. *Journal of Geophysical Research*, *114*, E10006. <https://doi.org/10.1029/2009JE003358>
- Krasnopolsky, V. A. (2002). Mars' upper atmosphere and ionosphere at low, medium, and high solar activities: Implications for evolution of water. *Journal of Geophysical Research*, *107*(E12), 5128. <https://doi.org/10.1029/2001je001809>
- Krasnopolsky, V. A. (2010). Solar activity variations of thermospheric temperatures on Mars and a problem of CO in the lower atmosphere. *Icarus*, *207*, 638.
- Laher, R. R., & Gilmore, F. R. (1990). Updated excitation and ionization cross sections for electron impact on atomic oxygen. *Journal of Physical and Chemical Reference Data*, *19*, 277.
- Lillis, R. J., Deighan, J., Fox, J. L., Bougher, S. W., Lee, Y., Combi, M. R., et al. (2017). Photochemical escape of oxygen from Mars: First results from MAVEN in situ data. *Journal of Geophysical Research: Space Physics*, *122*, 3815–3836. <https://doi.org/10.1002/2016JA023525>
- Mahaffy, P. R., Mahaffy, P., Benna, M., King, T., Harpole, D., Arvey, R., et al. (2015). The neutral gas and ion mass spectrometer on the Mars atmosphere and volatile evolution mission. *Space Science Reviews*, *195*, 49.
- Masuoka, T. (1994). Single- and double-photoionization cross sections of carbon dioxide (CO<sub>2</sub>) and ionic fragmentation of CO<sub>2</sub><sup>+</sup> and CO<sub>2</sub><sup>2+</sup>. *Physical Review A*, *50*, 3886.
- Masuoka, T., & Nakamura, E. (1993). Single-, double-, and triple-photoionization cross sections of carbon monoxide (CO) and ionic fragmentation of CO<sup>+</sup>, CO<sup>2+</sup>, and CO<sup>3+</sup>. *Physical Review A*, *48*, 4379.
- Mitchell, D. L., Lin, R. P., Mazelle, C., Rème, H., Cloutier, P. A., Connerney, J. E. P., et al. (2001). Probing Mars' crustal magnetic field and ionosphere with the MGS Electron Reflectometer. *Journal of Geophysical Research*, *106*, 23,419–23,427. <https://doi.org/10.1029/2000JE001435>
- Mitchell, D. L., Mazelle, C., Sauvaud, J.-A., Thocaven, J.-J., Rouzaud, J., Fedorov, A., et al. (2016). The MAVEN solar wind electron analyzer. *Space Science Reviews*, *200*, 495.
- Morgan, D. D., Gurnett, D. A., Kirchner, D. L., Fox, J. L., Nielsen, E., & Plaut, J. J. (2008). Variation of the Martian ionospheric electron density from Mars Express radar soundings. *Journal of Geophysical Research*, *113*, A09303. <https://doi.org/10.1029/2008JA013313>
- Mukundan, V., Thampi, S. V., Bhardwaj, A., & Krishnaprasad, C. (2020). The dayside ionosphere of Mars: Comparing a one-dimensional photochemical model with MAVEN Deep Dip campaign observations. *Icarus*, *337*(113502).
- Sakai, S., Andersson, L., Cravens, T. E., Mitchell, D. L., Mazelle, C., Rahmati, A., et al. (2016). Electron energetics in the Martian dayside ionosphere: Model comparisons with MAVEN data. *Journal of Geophysical Research: Space Physics*, *121*, 7049–7066. <https://doi.org/10.1002/2016JA022782>
- Sakai, S., Sakai, S., Rahmati, A., Mitchell, D. L., Cravens, T. E., Bougher, S. W., et al. (2015). Model insights into energetic photoelectrons measured at Mars by MAVEN. *Geophysical Research Letters*, *42*, 8894–8900. <https://doi.org/10.1002/2015GL065169>
- Slipski, M., Jakosky, B. M., Benna, M., Elrod, M., Mahaffy, P., Kass, D., et al. (2018). Variability of Martian turbopause altitudes. *Journal of Geophysical Research: Planets*, *123*, 2939–2957. <https://doi.org/10.1029/2018JE005704>
- Stammes, K., & Rees, M. H. (1983). Heating of thermal ionospheric electrons by suprathermal electrons. *Geophysical Research Letters*, *10*, 309–312.
- Stevens, M. H., Siskind, D. E., Scott Evans, J., Fox, J. L., Deighan, J., Jain, S. K., & Schneider, N. M. (2019). Detection of the nitric oxide dayglow on Mars by MAVEN/IUVS. *Journal of Geophysical Research: Planets*, *124*, 1226. <https://doi.org/10.1029/2019JE005945>
- Stolte, W. C., He, Z. X., Cutler, J. N., Lu, Y., & Samson, J. A. R. (1998). Dissociative photoionization cross sections of N<sub>2</sub> and O<sub>2</sub> from 100 to 800 eV. *Atomic Data and Nuclear Data Tables*, *69*, 171.
- Stone, S. W., Yelle, R. V., Benna, M., Elrod, M. K., & Mahaffy, P. R. (2018). Thermal structure of the Martian upper atmosphere from MAVEN NGIMS. *Journal of Geophysical Research: Planets*, *123*, 2842–2867. <https://doi.org/10.1029/2018JE005559>
- Thiemann, E. M. B., Chamberlin, P. C., Eparvier, F. G., Templeman, B., Woods, T. N., Bougher, S. W., & Jakosky, B. M. (2017). The MAVEN EUVM model of solar spectral irradiance variability at Mars: Algorithms and results. *Journal of Geophysical Research: Space Physics*, *122*, 2748–2767. <https://doi.org/10.1002/2016JA023512>
- Verner, D. A., Ferland, G. J., Korista, K. T., & Yakovlev, D. G. (1996). Atomic data for astrophysics. II. New analytic FITS for photoionization cross sections of atoms and ions. *The Astrophysical Journal*, *465*, 487.
- Wellbrock, A., Coates, A. J., Sillanpaa, I., Jones, G. H., Arridge, C. S., Lewis, G. R., et al. (2012). Cassini observations of ionospheric photoelectrons at large distances from Titan: Implications for Titan's exospheric environment and magnetic tail. *Journal of Geophysical Research*, *117*, A03216. <https://doi.org/10.1029/2011JA017113>
- Wu, X.-S., Cui, J., Cao, Y.-T., Liu, L.-J., Zhou, Z.-J., Huang, Y.-Y., et al. (2019). On the Hardness of the Photoelectron Energy Spectrum Near Mars. *Journal of Geophysical Research: Planets*, *124*, 2745–2753. <https://doi.org/10.1029/2019JE006093>
- Wu, X.-S., Cui, J., Cao, Y.-T., Sun, W.-Q., Luo, Q., & Ni, B.-B. (2019). Response of photoelectron peaks in the Martian ionosphere to solar EUV/X-ray irradiance. *Earth and Planetary Physics*, *4*(4), 1–6. <https://doi.org/10.26464/epp2020035>
- Xu, S., Liemohn, M., Bougher, S., & Mitchell, D. (2016). Martian high-altitude photoelectrons independent of solar zenith angle. *Journal of Geophysical Research: Space Physics*, *121*, 3767–3767. <https://doi.org/10.1002/2015JA022149>
- Xu, S., Mitchell, D., Liemohn, M., Fang, X., Ma, Y., Luhmann, J., et al. (2017). Martian low-altitude magnetic topology deduced from MAVEN/SWEA observations. *Journal of Geophysical Research: Space Physics*, *122*, 1831–1852. <https://doi.org/10.1002/2016JA023467>
- Yao, M., Cui, J., Wu, X., Huang, Y., & Wang, W. (2019). Variability of the Martian ionosphere from the MAVEN Radio Occultation Science Experiment. *Earth and Planetary Physics*, *3*, 283.